American Journal of
Biomedical Science & Research

www.biomedgrid.com
ISSN: 2642-1747

Research Article

O-HA Accelerates Skin Wound Healing in Mice by Enhancing Fibroblast Proliferation and Antioxidant Capacity

Bo Dou[1,2#], Shaoyuan Huang[2#], Ruiqi Wu[3], Xueli Su[2], Chang Liang[2], Yanru Zhu[2], Changhua Hu[1*] and Xiaoqun Duan[2*]

[1]*School of Pharmaceutical Sciences, Medical Research Institute, Southwest University, Chongqing, China*

[2]*School of Pharmacy, Guilin Medical University, Guilin, Guangxi, China*

[3]*Guangzhou Bay Area Institute of Biomedicine, Guangdong Lewwin Pharmaceutical Research Institute Co., Ltd., Guangdong Provincial Key Laboratory of Drug Non-Clinical Evaluation and Research, Guangzhou, China*

***Corresponding author:** Xiaoqun Duan and Changhua Hu, School of Pharmacy, Guilin Medical University, Guilin, Guangxi, China. School of Pharmaceutical Sciences, Medical Research Institute, Southwest University, Chongqing, China.

To Cite This article: *Bo Dou#, Shaoyuan Huang#, Ruiqi Wu, Xueli Su, Chang Liang, Yanru Zhu, Changhua Hu* and Xiaoqun Duan*, O-HA Accelerates Skin Wound Healing in Mice by Enhancing Fibroblast Proliferation and Antioxidant Capacity. Am J Biomed Sci & Res. 2026 32(2) AJBSR.MS.ID.004136,* **DOI:** 10.34297/AJBSR.2026.32.004136

Received: August 21, 2026 **Published:** September 09, 2026

Abstract

In recent years, various biomaterials based on Hyaluronic Acid (HA) have shown considerable promise for tissue repair, with their efficacy influenced by molecular weight. In this study, hyaluronidase (HAase) was employed to enzymatically hydrolyze hyaluronic acid, resulting in the production of several Hyaluronic Acid Oligosaccharides (o-HA) with weight-average Molecular Weights (Mw) ranging from 2.8 to 40 kDa. Subsequently, we evaluated the effects of these o-HA on 3T3 and L929 cells. The results indicated that HA3 (Mw 9.9 kDa) promoted the proliferation and improved scratch closure of 3T3 cells, while HA4 (Mw 4.1 kDa) had the same effect on L929 cells. Both fragments alleviated oxidative damage induced by UVB irradiation. Furthermore, an animal wound model was used to verify the impact of o-HA in the 4.1-9.9 kDa range on wound healing. We found that o-HA within this molecular weight range enhanced epithelial regeneration and collagen deposition in C57BL mice. Western blot analysis revealed that after o-HA treatment, the expression levels of skin-healing-related proteins such as Collagen I, TGF-β1, and VEGFA in the wound sites of C57BL mice increased. This effect may be associated with the activation of the PI3K cell signaling pathway.

Keywords: Hyaluronic acid oligosaccharides, Antioxidant, Wound healing

Introduction

Wound healing is a multifaceted physiological process whose duration depends on the type and extent of the injury [1]. Skin wounds caused by physical and chemical trauma pose a significant challenge to skin health. While epidermal and superficial wounds often regenerate on their own, deeper partial- and full-thickness wounds require prompt treatment to prevent infection and deformity [2]. The most common therapeutic approach is skin grafting, which includes autografts, allografts, and xenografts [3]. However, these methods have drawbacks and limitations: insufficient availability of grafts, rejection risks, skin infections,

and potential carcinogenesis [4,5]. Therefore, developing new and effective therapeutic agents and technologies is necessary.

Wound dressings are crucial for managing wound healing, protecting the wound from the environment, and speeding up the recovery process [6]. Many are fabricated from natural polymers, such as hyaluronic acid, alginate, cellulose, gelatin, and collagen7. These natural polymers offer beneficial wound-healing properties, including bioactivity, biocompatibility, and biodegradability [7]. Recently, Hyaluronic Acid (HA) based biomaterials have shown great potential for modulating inflammatory responses, promoting angiogenesis, and aiding tissue repair [8,9]. The role of HA in managing oxidative stress and inflammation has been applied in treating chronic inflammatory diseases, including osteoarthritis and inflammatory bowel disease [10]. Ongoing research into the complex roles of HA in health and disease continues to broaden its biomedical applications, suggesting new strategies for improving wound healing and tissue regeneration [8].

HA is a linear glycosaminoglycan polymer composed of alternating (β,1–4)-glucuronic acid (GlcA) and (β,1–3)-N-acetylglucosamine (GlcNAc) disaccharide units [11]. Its molecular mass can range from several thousand to millions of Daltons [12]. The biological activity of HA varies with its molecular weight, due to differences in its distribution, metabolic fate, and interactions with cellular receptors. High-molecular-weight HA ($Mw>2\times10^6$) demonstrates properties like good viscoelasticity, moisturizing capacity, and anti-inflammatory effects. HA with a Mw between 1×10^6 and 2×10^6 offers benefits such as moisturizing, lubrication, and sustained drug release. o-HA, particularly those with a molecular weight below 1×10^4 Da or between 1×10^4 and 8×10^4 Da, demonstrate diverse functions such as antitumor effects, wound healing promotion, and stimulation of angiogenesis and bone formation [13-18]. Thus, clarifying the relationship between HA molecular weight and its bioactivity is crucial for advancing our understanding of related disease mechanisms and for developing improved therapeutic and biomaterial strategies, and optimizing biomedical materials. In this study, we employed hyaluronidase (HAase) enzymatic digestion to degrade HA (50 kDa) into o-HA fragments with Mw ranging from 2.8-40 kDa. Through in vitro and in vivo experiments, we analyzed the impact of these HAase-derived o-HA fragments on wound healing in mice.

Instruments and Materials

The following materials were used in this study: HAase (Source of bovine testes, 300 IU/mL, Beijing Solarbio, China). HA (Source of *Streptococcus*, 50 kDa, Batch number: BL20240116001, Shaanxi Bolin Biotechnology, China). Mouse fibroblast cells (L929) and mouse embryonic fibroblast cells (3T3) were obtained from the Shanghai Cell Bank of the Chinese Academy of Sciences. Superoxide Dismutase Detection Kit (SOD), Glutathione Peroxidase Detection Kit (GSH-Px), Catalase Detection Kit (CAT), and Malondialdehyde Detection Kit (MDA) were purchased from Nanjing Jiancheng Bioengineering Institute in China. Cell culture reagents including Dulbecco's Modified Eagle Medium (DMEM), phosphate-buffered saline (PBS), penicillin/streptomycin, trypsin, and Fetal Bovine Serum (FBS) were supplied by Thermo Fisher Scientific (Gibco, Grand Island, NY, USA). The antibodies were purchased from Affinity Biosciences Co., Ltd. (Shanghai, China; TGF-β1, Cat#: DF8001; VEGFA, Cat#: DF8002), Proteintech Group, Inc. (Wuhan, China; Collagen I, Cat#: 11270-1-AP), and Cell Signaling Technology, Inc. (Massachusetts, United States; PI3K, Cat#: 4250; p-PI3K, Cat#: 4251; GAPDH, Cat#: 4971; β-Actin, Cat#: 4972). The primary antibody dilution buffer (Cat#: P0203) and secondary antibody dilution buffer (Cat#: P0208) were obtained from Beyotime Biotechnology Co., Ltd. (Shanghai, China). All other chemical reagents were purchased from (Shanghai Aladdin, China). Optical measurements were carried out using a UV-2100 spectrophotometer (Unico, China). ELx800 Epoch Full-Waveband Multi-Function Enzyme-Labeling (Biotek, USA). The high-performance liquid chromatography (HPLC) system (Model 1260 Infinity II) equipped with a refractive index detector (RID) was purchased from Agilent Technologies, Inc. (Santa Clara, California, USA). The analytical columns used were Waters Ultrahydrogel 1000 and Waters Ultrahydrogel 120 in series (Waters Corporation, Milford, Massachusetts, USA). Q Exactive Orbitrap mass spectrometer (Thermo Fisher Scientific, Waltham, Massachusetts, USA). Inverted fluorescence microscope (Guangzhou Mingmei Optoelectronic Technology, China).

Methods

Enzymatic Degradation of HA And Molecular Weight Determination

HA (50 kDa) was digested with HAase (300 IU/mL) at an enzyme-to-substrate mass-to-volume ratio of 1:100 (w/v) at 25 °C for different durations:1 min (HA1), 5 min (HA2), 10 min (HA3), 30 min (HA4), 60 min (HA5), and 120 min (HA6). After digestion for a specified period, raise the reaction temperature to 100°C to terminate the reaction. The molecular weight profiles of the resulting HA fragments were analyzed by Gel Permeation Chromatography (GPC) [19]. A differential Refractive Index Detector (RID) was used for monitoring, obtaining the number-average Molecular Weight (Mn), weight-average Molecular Weight (Mw), and molecular weight distribution [19]. Mobile phase: 0.1 M $NaNO_3$ solution; Flow rate: 0.8 mL/min; Temperature: 40°C. Dextran standards with molecular weights of 401,300 Da, 123,600 Da, 43,500 Da, 9,890 Da, and 4,440 Da were used to create a standard curve. Data were plotted using Origin software.

Effect Of Different O-HA Molecular Weights On 3T3 And L929 Cell Viability

3T3 and L929 cell suspensions were seeded into 96-well plates at a density of 1.5×10^4 cells/well and incubated at 37°C with 5% CO_2 for 24 h. Following cell attachment, the medium was replaced. Cells in the control group were treated with undegraded HA (50 kDa), whereas treatment groups received HA1 through HA6 at concentrations ranging from 10 to 80 μg/mL. After 24 h of further

culture, 10 μL of CCK-8 solution (Dojindo, Japan) was added to each well (final dilution of 1:10, i.e., 10% v/v in the culture medium), and the plates were returned to the incubator for 30 min. The absorbance (OD value) is measured at 450 nanometers using a microplate reader to calculate cell viability, and the calculation formula is Ep. (1) [20].

$$\text{Cell Viability (\%)} = (\text{OD\_treatment} / \text{OD\_control}) \times 100\% \quad (1)$$

Effect of HA3 and HA4 on 3T3 and L929 cell scratch closure

Based on the outcomes of cell viability assays, HA3 at concentrations of 20, 40, and 60 μg/mL was selected to investigate its effect on the improved scratch closure of 3T3 cells, while HA4 at concentrations of 40, 60, and 80 μg/mL was chosen to evaluate its effect on the improved scratch closure of L929 cells. Prior to cell seeding, reference lines were drawn on the underside of 6-well plates to standardize image analysis across the later time points. 3T3 and L929 cells in the logarithmic growth phase were then seeded at a density of 3×10^5 cells/well and cultured at 37°C with 5% CO_2 for 24 h. After cell attachment, the cells were washed with PBS [20]. Three evenly spaced scratches were made perpendicular to the reference lines in each well using a sterile 200 μL pipette tip [21]. The wells were washed three times with PBS to remove cell debris and ensure clean scratch edges. The control group received serum-free medium. The 3T3 treatment groups received HA3 (20, 40, 60 μg/mL), and the L929 treatment groups received HA4 (40, 60, 80 μg/mL). Images of the scratch wounds were taken immediately (t=0 h) and again after 24 h of treatment (t=24 h) using an inverted microscope. Scratch areas were measured using ImageJ software to calculate the cell scratch closure rate for each group according to Eq. (2).

$$\text{Cell Migration Rate (\%)} = [(\text{Area\_t0} - \text{Area\_t24}) / \text{Area\_t0}] \times 100\% \quad (2)$$

Evaluate The Effects of HA3 And HA4 On 3T3 And L929 Cells, Respectively, That Have Undergone UVB-Induced Oxidative Damage

Based on the previous results of cell viability and migration, the effects of HA3 and HA4 on oxidative damage in 3T3 and L929 cells were evaluated. Oxidative stress and aging models were established by inducing 3T3 and L929 cells with UVB. Cells were seeded in 96-well plates at a density of 1.5×10^4 cells/well. After 12 h of culture for cell attachment, the culture medium was discarded, and the cells were washed three times with PBS. Then, the cells were starved in serum-free DMEM for 4 h to synchronize the cell cycle. In the experimental group, 100 μL of PBS was added to each well, and the cells were irradiated with 120 mJ/cm^2 UVB for 5 min; the control group was not irradiated, and the rest of the operations were the same. After irradiation, the control group was supplemented with serum-containing DMEM medium, the UVB group with serum - free DMEM medium, the 3T3-treated group with DMEM medium containing HA3 (20, 40, 60 μg/mL), and the L929-treated group with DMEM medium containing HA4 (40, 60, 80 μg/mL). Each group had 6 replicate samples. After further culturing for 24 h, DCFH-DA staining solution was added to each well and incubated at 37°C for 20-30 min. After washing the cells twice with PBS, the cells were observed and photographed under a fluorescence microscope. DCFH-DA reacts with ROS to form highly fluorescent DCF, the fluorescence intensity of which (typically at excitation/emission wavelengths of 488 nm/525 nm) is directly proportional to the intracellular ROS level, thereby enabling quantitative analysis of ROS content [22].

Effect Of HA3 And HA4 On Intracellular SOD, GSH-Px, CAT, And MDA Levels In 3T3 And L929 Cells, Respectively

3T3 and L929 cells were seeded in 6-well plates at a density of 3×10^5 cells/well and cultured for 24 h at 37°C with 5% CO_2. Cells were assigned to the same treatment groups described in Section 2.4 (normal, UVB model, and HA3/HA4 treatment), with three replicate wells per condition. After 24 h of further culture, cell samples from each group were collected for detection of oxidative stress indicators: SOD, GSH-Px, CAT, and MDA [22,23].

Preparation Of Skin Wound Model and Group Administration in C57BL Mice

Male C57BL mice aged 6–8 weeks with a body weight of 25±3 g were selected for the present study. All mice were Specific Pathogen-Free (SPF) grade, with the animal use license number SCXK(Yu)2020-0005, and were obtained from Henan Skobes Biotechnology Co., Ltd. All animal procedures received approval from the Guilin Medical University Animal Ethics Committee. Mice were anesthetized via intraperitoneal injection of a mixture of ketamine (80 mg/kg) and xylazine (10 mg/kg). Hair on the dorsal skin was removed. The midline of the back was marked, and a full-thickness skin wound 8 mm in diameter was created on the midline using a biopsy punch (Day 0) [20-22]. Utilize the C57BL mouse wound model to evaluate the effect of o-HA (Mw 4.1-9.9 kDa) on wound healing. After lyophilizing HA3 (Mw 9.9 kDa) and HA4 (Mw 4.1 kDa), they are mixed at a weight ratio of 1:1. Subsequently, mixed o-HA viscous solution of different concentrations were prepared (o-HA 0.5 mg/mL: 50 mg mixed o-HA+100 mL saline; o-HA 1 mg/mL: 100 mg mixed o-HA+100 mL saline; o-HA 2 mg/mL: 200 mg mixed o-HA+100 mL saline). The mice were randomly divided into six groups, with six mice in each group: normal control, model group (washed daily with saline), positive drug group (topical application of Yunnan Baiyao), and three o-HA groups (o-HA 0.5 mg/mL, 1 mg/mL, 2 mg/mL). The different o-HA viscous solutions were applied topically to the wound area (approx. 1 cm^2) twice daily. Wounds were photographed every two days for observation.

Histological Analysis

On day 7, mice were anesthetized via intraperitoneal injection of a mixture of ketamine (80 mg/kg) and xylazine (10 mg/kg), and

were subsequently sacrificed by cervical dislocation. Skin wound tissues and major organs (heart, liver, spleen, lungs, and kidneys) were harvested for histological assessment of healing and biosafety. Tissues were fixed in 4% paraformaldehyde for 24 h, embedded in OCT compound (Sakura Finetek USA), and sectioned at 10 μm [24]. Sections were stained with Hematoxylin and Eosin (H&E) to examine general pathological and physiological states of skin wounds and organs. Masson's trichrome staining was performed to assess total collagen accumulation [24]. Morphological changes in skin tissue were examined using an optical microscope, and images were captured.

Analyze The Impact Of O-HA On Wound Healing-Related Proteins in C57BL Mice Through Western Blot

Total protein was isolated from wound bed tissues of each treatment group for immunoblotting analysis. Proteins were separated on SDS-PAGE (10%) gels and transferred onto PVDF membranes (Millipore, Germany). After blocking with 5% BSA for 2 h at room temperature, membranes were incubated overnight at 4°C with primary antibodies against TGF-β1, VEGFA, Collagen I, PI3K, and p-PI3K (diluted 1:1000) [25]. Following washes, membranes were incubated with HRP-conjugated secondary antibodies (1:1000 dilution) for 1 h at room temperature. Blots were developed using chemiluminescent reagent. GAPDH and β-Actin served as internal controls. Expression levels of target proteins relative to GAPDH and β-Actin were analyzed via grayscale value analysis using ImageJ software.

Statistical Analysis

All the data are presented as the mean ± Standard Deviation (SD) of three independent experiments. Two-tailed Student's t test and one-way analysis of variance (ANOVA) followed by Tukey's post-hoc test for multiple comparisons were used for group comparisons using GraphPad Prism 10.0 (GraphPad Software, San Diego, CA, USA). Variance homogeneity was checked using Levene's test before applying ANOVA. A P value < 0.05 was considered statistically significant.

Results and Discussion

Determination Of Molecular Weight and Distribution of Degraded HA By GPC

The molecular weight of HA is often determined using methods like agarose gel electrophoresis, viscometry, and Gel Permeation Chromatography (GPC) [26]. However, agarose gel electrophoresis offers only a rough estimate and lacks precision [27]. Viscometry yields relative molecular mass values that are significantly influenced by the inner diameter of the Ubbelohde viscometer and temperature. Furthermore, the unique viscoelasticity of HA means no perfect standard exists, so analysts often rely on structurally similar polysaccharides for calibration, potentially affecting accuracy [26,28]. GPC is a technique within liquid chromatography that separates polymer samples based on molecular weight distribution using a stationary phase of porous gel particles with varying pore sizes [26,28]. As a solution of polymer molecules passes through the column, larger molecules are excluded from the gel pores and elute first. Smaller molecules penetrate the pores to varying degrees, causing them to elute later, in order of decreasing size [28]. Using GPC, we clearly determined the average molecular weight and distribution profile of each o-HA sample. As shown in Figure 1 and Table 1: after 1 min of degradation, HA1 had an Mw around 40 kDa; after 5 min, HA2 ~ 11 kDa; after 10 min, HA3~9.9 kDa; after 30 min, HA4~4.1 kDa; after 60 min, HA5~2.8 kDa. Unfortunately, for HA6 degraded for 120 min, the molecular weight was too small to be determined accurately (Figure 1) (Table 1).

Table 1: Molecular weight and distribution of o-HA determined by GPC.

o-HA	Number-average molecular weight (Mn)	Weight-average molecular weight (Mw)	Molecular weight distribution (Mw/Mn)
HA1	1297	40218	31.009
HA2	1203	11187	9.299
HA3	1191	9900	8.312
HA4	992	4144	4.177
HA5	882	2871	3.255

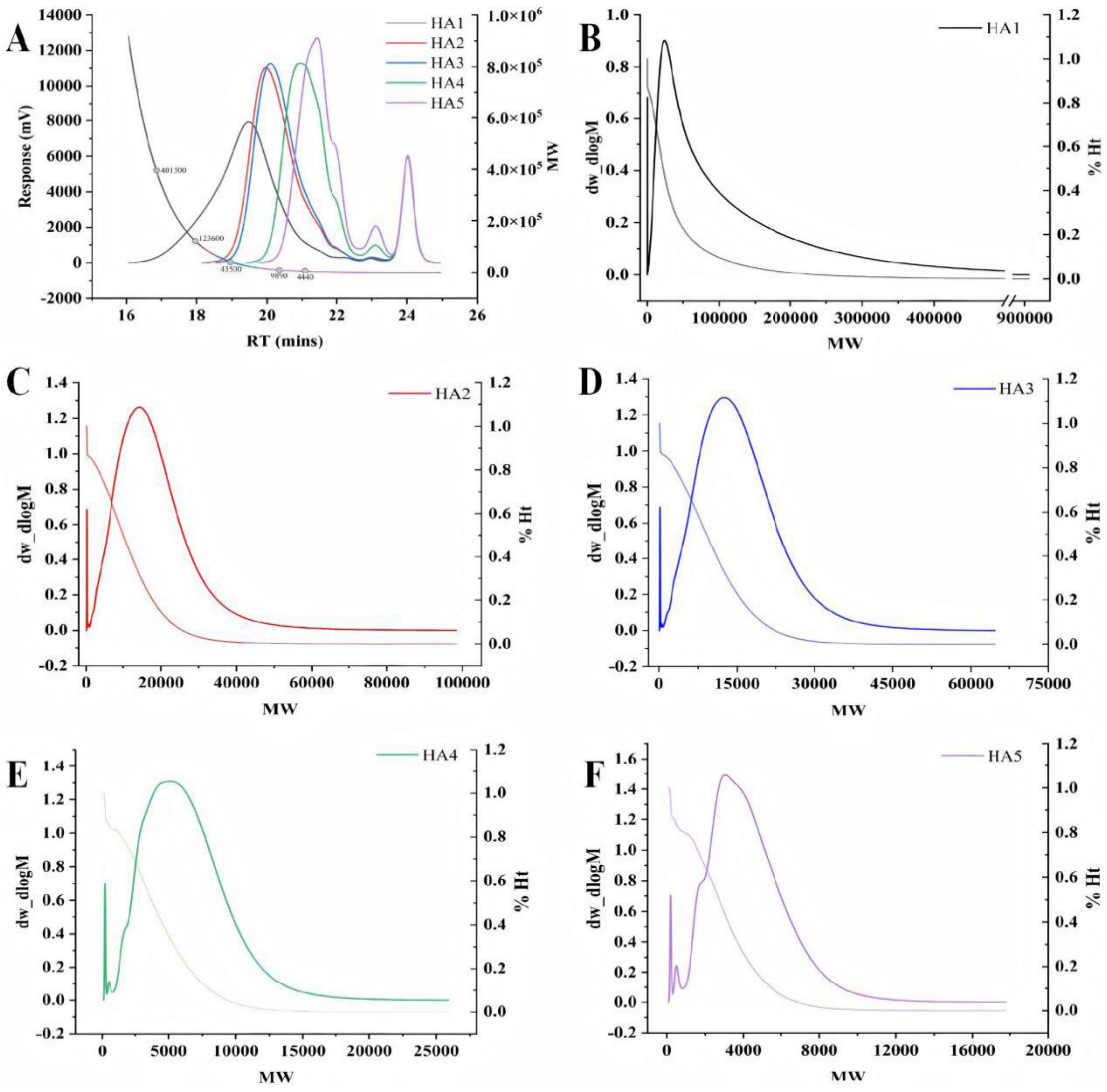

Figure 1: Elution curves and molecular weight distribution of HA after degradation. (A): Elution curves of HA1-HA5 after HA degradation. (B): Molecular weight distribution of HA1. (C): Molecular weight distribution of HA2. (D): Molecular weight distribution of HA3. (E): Molecular weight distribution of HA4. (F): Molecular weight distribution of HA5.

Effects Of Six Types Of O-HA (HA1 - HA6) On the Viability Of 3T3 And L929 Cells

Studies show that HA with a molecular weight around 5 kDa, when incorporated into chitosan hydrogels can significantly improve the adhesion, growth, and proliferation of L929 cells [29]. *Goldberg RL et al*. found that high-molecular-weight HA markedly inhibited 3T3 cell proliferation, an effect that weakened as the HA molecular size decreased [30]. These findings align with our results. Using the CCK-8 assay, we evaluated how HAase-degraded o-HA affected the viability of 3T3 and L929 cells. As shown in (Figure 2), undegraded HA (Mw 50 kDa) had no significant effect on either cell type. In contrast, HAase-degraded fragments HA1 through HA4 (Mw 40-4.1 kDa) significantly enhanced 3T3 cell viability. HA3 (Mw 9.9 kDa) produced the most pronounced effect. For L929 cells, HA3, HA4, and HA5 (Mw 9.9-2.8 kDa) significantly boosted cell viability, with HA4 (Mw 4.1 kDa) demonstrating the strongest effect (Figure 2).

Effect of HA3 and HA4 on the scratch closure of 3T3 and L929 Cells

o-HA with a molecular weight of 800-1500 Da can significantly enhance human keratinocyte scratch closure by activating the HIF-1α/VEGFA signaling pathway [31]. Furthermore, *Giometti C F et al.* reported that culturing 3T3 cells in HA-supplemented hydrogels led to a significant increase in cell growth, highlighting HA's potential as a biomaterial for tissue regeneration [32]. Given that HA3 (Mw 9.9 kDa) and HA4 (Mw 4.1 kDa) enhanced the viability of 3T3 and L929 cells respectively (Figure 2), we further conducted a scratch assay to evaluate the effects of HA3 and HA4 on the scratch closure

of 3T3 and L929 cells. The results in Figure 3A show consistent scratch areas at 0 h. After 24 h of HA3 intervention, a notably larger scratch closure area and a narrower scratch width were observed for 3T3 cells, with the effect becoming more apparent at higher concentrations. Figure 3B demonstrates HA4's effect on L929 cell scratch closure. After 24 h of treatment, the cell scratch closure rate increased significantly compared to the control and exhibited a concentration-dependent rise with increasing HA4 doses. These results confirm that HAase-derived o-HA in the 4.1-9.9 kDa range promotes properties critical for wound healing (Figure 3).

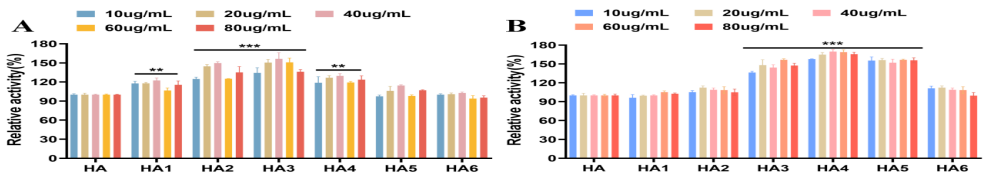

Figure 2: Effect of different o-HA molecular weights and concentrations on viability (A) 3T3 cells viability (B) L929 cells viability. n=3. Compared with undegraded HA: **P<0.01, ***P<0.001.

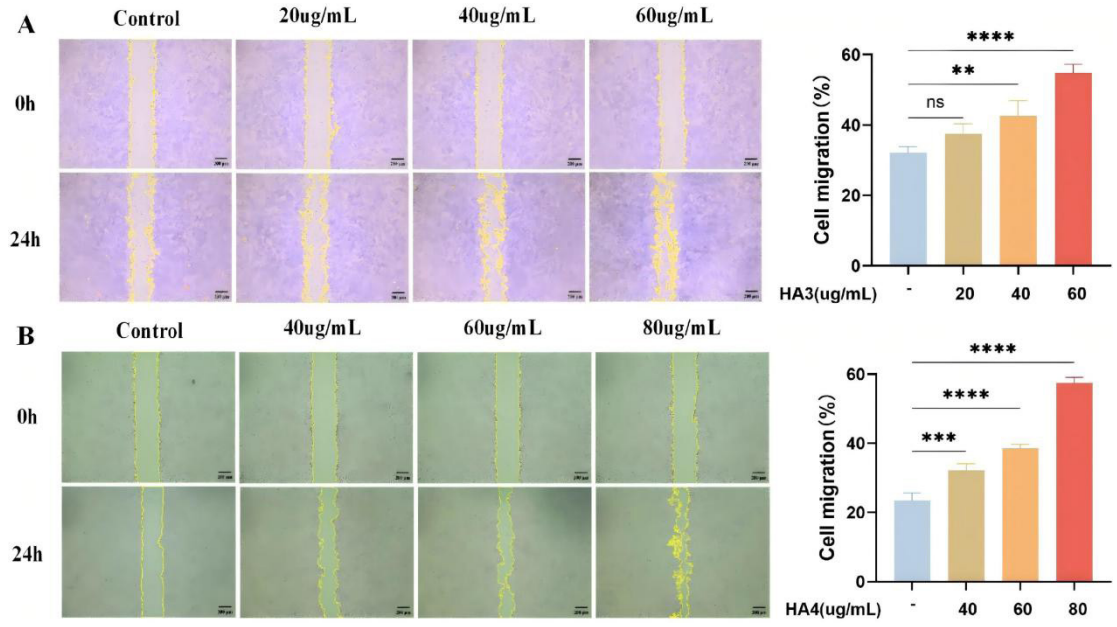

Figure 3: Effect of o-HA on cell scratch closure. (A) Effect of HA3 on 3T3 cell migration. (B) Effect of HA4 on L929 cell migration. n=3. Compared with the blank control group: **P<0.05, ***P<0.01,****P<0.001.

Effect Of HA3 And HA4 On Oxidative Damage In 3T3 And L929 Cells

Liu J et al. [33] reported that HA (~30.8 kDa) could reduce cellular oxidative stress by lowering hypoxia-induced reactive oxygen species (ROS) levels. DCFH-DA reacts with ROS to form highly fluorescent DCF, the fluorescence intensity of which is directly proportional to the intracellular ROS level [22]. We employed the DCFH-DA probe to stain the cells, evaluated the repair effect of HA3 on UVB-induced oxidative damage in 3T3 cells. As shown in Figure 4A, compared with the control group, UVB induction increased the intracellular ROS production. After 24 hours of intervention with different concentrations of HA3 (20, 40, 60 μg/mL), the ROS level in 3T3 cells gradually decreased with the increase of HA3 concentration. Additionally, we investigated the oxidative damage of L929 cells after UVB irradiation treated with HA4. The results in Figure 4B indicated that a large amount of ROS was produced in L929 cells after UVB irradiation. After 24 hours of intervention with HA4, the intracellular ROS decreased with the increase of HA4 concentration (Figure 4).

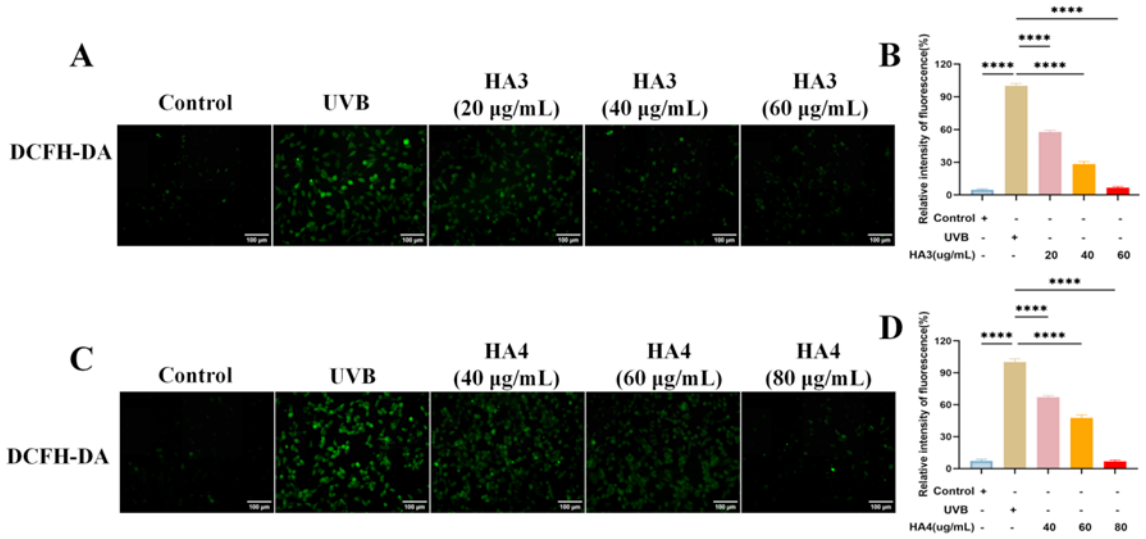

Figure 4: The effects of HA3 and HA4 on ROS in 3T3 and L929 cells after UVB-induced oxidative damage (A) Fluorescence staining images of 3T3 cells (B) Relative fluorescence intensity of 3T3 cells (C) Fluorescence staining images of L929 cells. (D) Relative fluorescence intensity of L929 cells. n=3. Compared with UVB group, ****P<0.0001.

Effect of HA3 and HA4 on Intracellular SOD, GSH-Px, CAT, and MDA Levels in 3T3 and L929 Cells

The primary enzymatic antioxidant defense system, comprising superoxide dismutase (SOD), glutathione peroxidase (GSH-Px), and catalase (CAT), scavenges reactive oxygen species, maintaining the oxidant-antioxidant balance and protecting cells from oxidative stress damage [34,35]. Malondialdehyde (MDA) is a product of lipid peroxidation degradation. Its concentration reflects the degree of lipid peroxidation and free radical levels in the body, indirectly indicating the extent of cellular damage [34,35]. We further assessed the antioxidant effects of HA3 and HA4 on UVB-irradiated 3T3 and L929 cells, respectively. The results in (Figure 5) show that compared to the normal group, UVB induction led to a significant decrease in intracellular SOD, GSH-Px, and CAT levels and an increase in MDA levels in both 3T3 and L929 cells. This indicates a disrupted oxidative balance and a state of oxidative stress. Intervention with HA3 and HA4 increased SOD, GSH-Px, and CAT levels while decreasing MDA levels in both cell types. These findings indicate that HA3 and HA4 bolster cellular antioxidant defenses, enhance free radical scavenging, and reduce lipid peroxidation. Low-molecular-weight HA has been shown to increase SOD and CAT activity in fibroblasts while lowering MDA levels, thereby reversing the cellular oxidative stress state [36]. Similarly, *Campo GM et al.* [37] reported that in an oxidative stress model of human dermal fibroblasts, HA effectively reduced hydroxyl radical (·OH) generation and DNA strand breaks while enhancing the activity of endogenous antioxidant enzymes like SOD and CAT, thus exerting a protective effect (Figure 5).

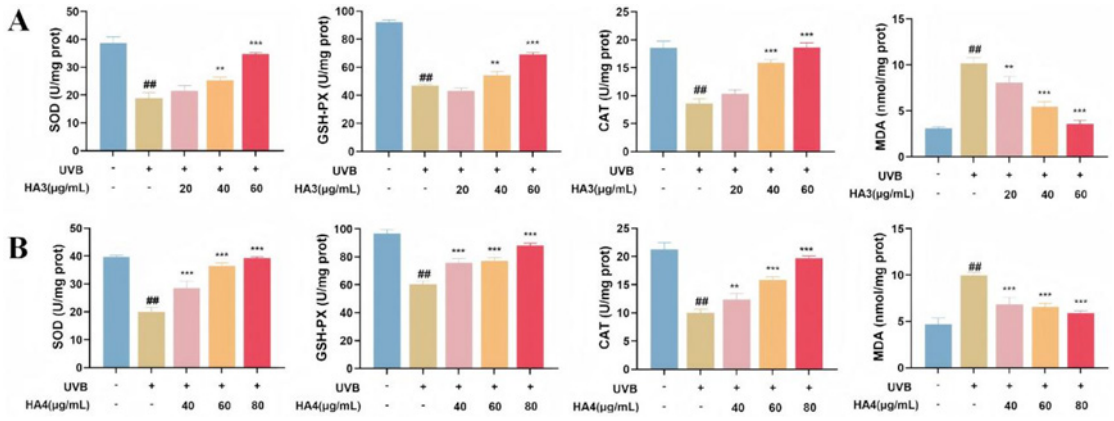

Figure 5: Effect of HA3 and HA4 on the antioxidant capacity of 3T3 and L929 cells. A: Effect of HA3 on SOD, GSH-Px, CAT, and MDA levels in 3T3 cells. B: Effect of HA4 on SOD, GSH-Px, CAT, and MDA levels in L929 cells. n=3. Compared with the control group: #P<0.05, ##P<0.01; Compared with UVB group, **P<0.01, ***P<0.001.

The effects of mixed o-HA at different concentrations on wound healing in C57BL mice

o-HA (Mw 35 kDa) can significantly improve L929 cell viability, which thus highlights it as a potential material for promoting skin wound healing [31,38]. Furthermore, *Gao Y et al.* [24] reported that low-molecular-weight HA (~39 kDa) accelerated the healing of full-thickness excisional skin wounds in mice by modulating the early inflammatory response, promoting epithelialization and neovascularization, and remodeling collagen. We evaluated the effect of o-HA viscous solution (HA3 and HA4; 4.1-9.9 kDa) on wound healing using a C57BL mouse model. Different concentrations of o-HA viscous solution were applied topically to wounds (approx. 1 cm^2) twice daily, with photographs taken every two days. Healing capacity was assessed on day 7. As shown in (Figure 6), the average wound closure rate in the model group was around 60%. Compared with the model group, the wound healing rate of the group treated with o-HA viscous solution was significantly increased, and the healing rate of the group treated with o-HA viscous solution at a concentration of 2 mg/mL was close to 95% (Figure 6).

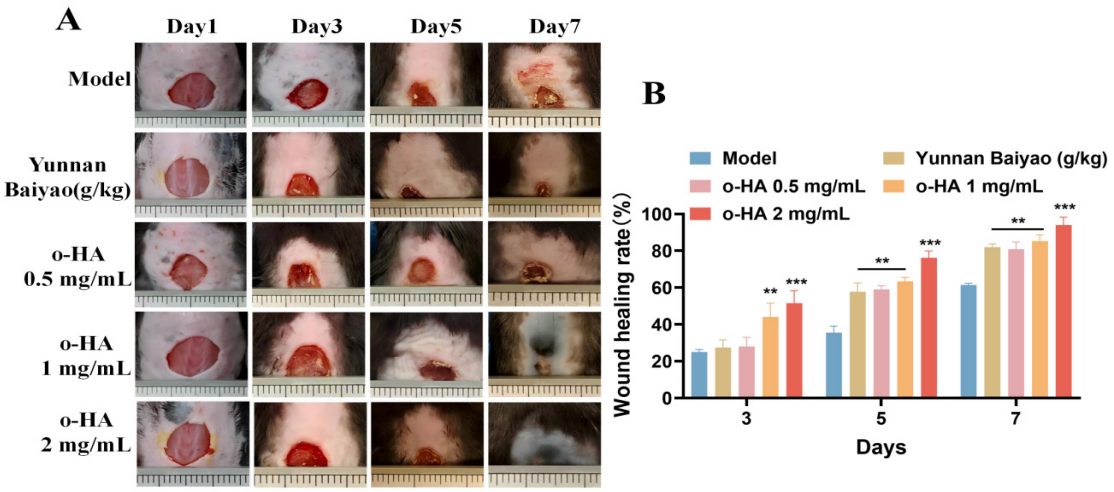

Figure 6: Effect of o-HA viscous solution on wound healing in mice. A: Representative wound images of each group during the period from model establishment to drug administration (Days 1, 3, 5, and 7). B: Quantitative graphs of wound healing rates during the period from model establishment to drug administration (3, 5, and 7 days) for each group. n=6. In comparison with the model group, **P<0.01, ***P<0.001.

Effect of o-HA viscous solution on the Histopathology of Wound Skin in C57BL Mice

In tissue repair, low-molecular-weight HA effectively promotes wound re-epithelialization and guides organized collagen deposition and remodeling, which accelerates the restoration of functional dermal structure [24,31,38]. As shown in (Figure 7), o-HA viscous solution treated wounds exhibited greater contraction and narrower granulation tissue compared to controls. Moreover, in the treatment group with the o-HA viscous solution at a concentration of 2 mg/mL, newly formed hair follicle tissues can be visually observed, and the newly formed epidermis is smooth and thin. Collagen is the main component of the skin and subcutaneous connective tissue matrix and is crucial for wound healing and restoring skin mechanical strength. Therefore, collagen deposition are key indicators for assessing wound healing quality [39,40]. Masson staining is also a commonly used method in pathological analysis, which mainly observes the types, distribution, and morphological characteristics of fibers in tissues. After staining, collagen fibers appear blue, while muscle fibers appear reddish-purple. During the wound healing process, collagen fibers will undergo varying degrees of expansion over time, which is also known as collagen deposition [40]. Therefore, by Masson staining results, the expression level of collagen fibers in the wound can be observed. The results indicate that the fiber arrangement in the model group is disordered and sparse. In contrast, both the positive drug group and the o-HA viscous solution group show different degrees of collagen deposition. In the 2 mg/mL o-HA viscous solution treatment group, a large amount of new collagen fibers have formed at the wound site. It was demonstrated that the o-HA viscous solution could effectively promote collagen deposition in skin wounds and facilitate wound healing (Figure 7).

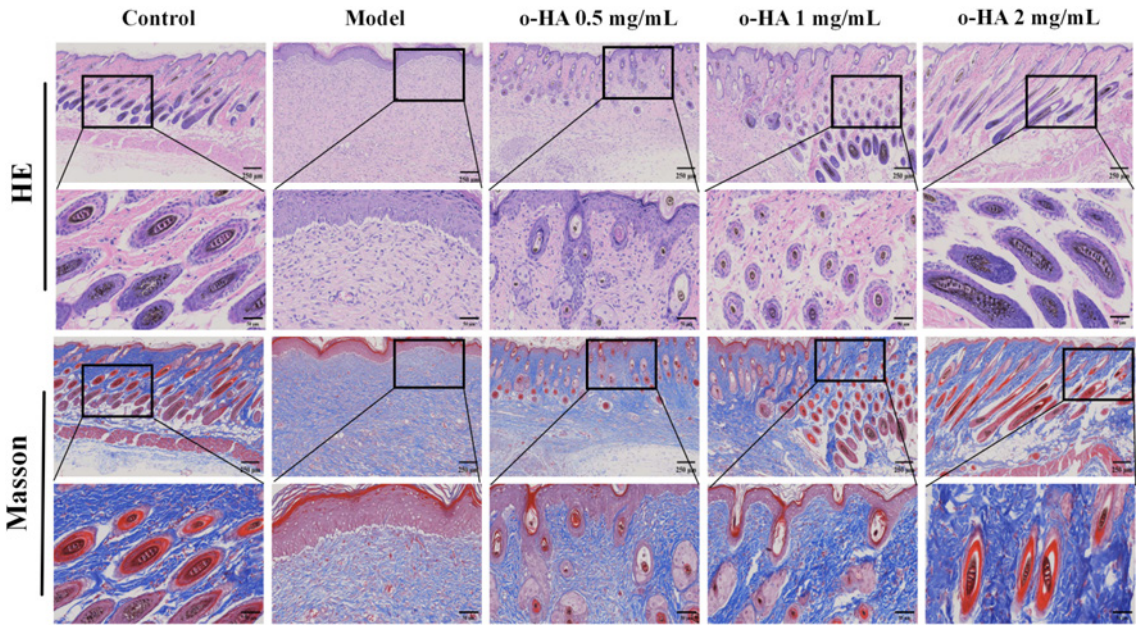

Figure 7: Effects of drug administration in each group on the histopathology of wound skin tissue in C57BL mice. HE staining: First row (scale bar: 250 μm), second row (scale bar: 50 μm); Masson staining: First row (scale bar: 250 μm), second row (scale bar: 50 μm).

Effects Of Each Group on the Histopathology of Major Visceral Organs in C57BL Mice

For clinical application, the in vivo biosafety of wound healing materials is essential [41]. We employed H&E staining to evaluate the influence of o-HA viscous solution on the histopathology of various organs in C57BL mice after treating their skin wounds. As shown in the (Figure 8), the o-HA viscous solution did not cause any significant histopathological abnormalities in the major organs (heart, liver, spleen, lungs, kidneys) of mice (Figure 8).

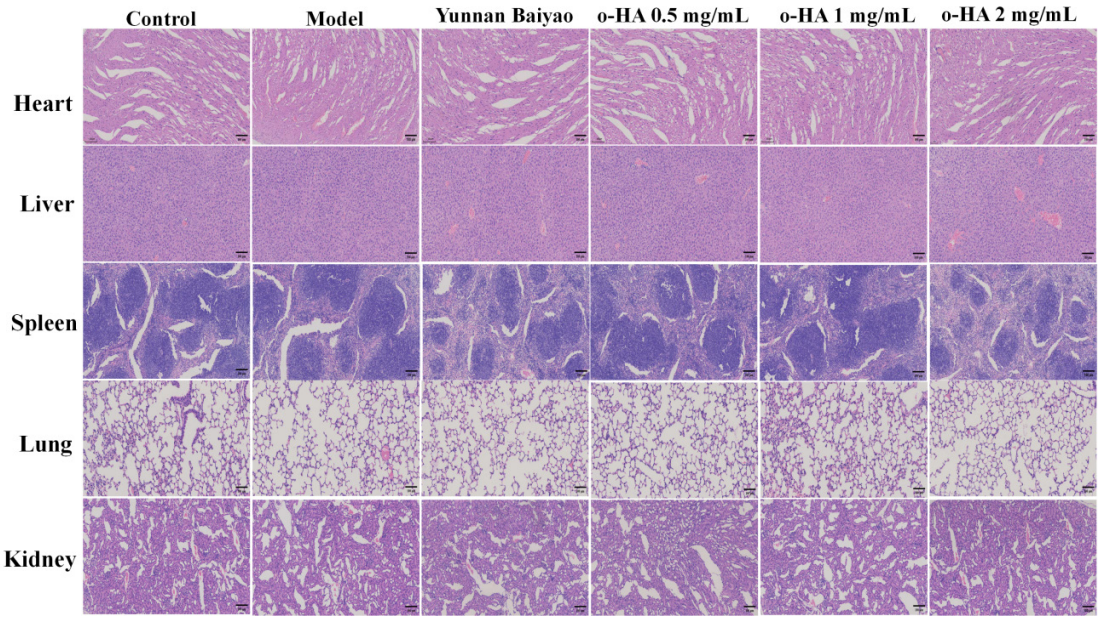

Figure 8: After the administration is completed, the effects of each group on the histopathology of the main organs (heart, liver, spleen, lung, and kidney) of C57BL mice. (scale bar: 100 μm).

Effect of o-HA on the Expression of PI3K, Collagen I, VEGFA, and TGF-β1 Proteins in Wound Skin of C57BL Mice

Studies indicate that accelerating skin wound healing involves promoting the proliferation and migration of cells such as dermal fibroblasts and endothelial cells, as well as enhancing vascular formation. This effect is achieved by upregulating the expression of proteins like TGF-β1 and Collagen I, and the underlying mechanism is confirmed to involve activation of the PI3K cell signaling pathway [42]. Thus, activation of the PI3K signaling pathway is associated with accelerated skin wound healing [43]. Furthermore, key factors in skin wound repair include collagen deposition, primarily driven by transforming growth factor-beta (TGF-β), and angiogenesis, mainly regulated by vascular endothelial growth factor (VEGF) [44,45]. Low-molecular-weight HA fragments can specifically upregulate the expression of Collagen I and TGF-β1 in fibroblasts and activate signaling pathways such as PI3K/Akt, thereby promoting cell proliferation and matrix remodeling to accelerate wound healing [46]. *Chen Y et al.* [47] found that HA hydrogels upregulated key factors like VEGF and its downstream PI3K/Akt signaling pathway, effectively promoting endothelial cell proliferation, migration, and tube formation to achieve angiogenesis. However, these studies did not specify the molecular weight of HA used. We analyzed the PI3K cell signaling pathway and the expression of skin healing-related proteins (Collagen I, TGF-β1, VEGFA) via immunoblotting. As shown in (Figure 9), compared with the model group and the positive control group, the expression levels of Collagen I, TGF-β1, and VEGFA in the o-HA viscous solution group increased with the increase in o-HA concentration. This indicates that the o-HA viscous solution can enhance the expression of skin healing proteins Collagen I, TGF-β1, and VEGFA during the skin healing process. Additionally, we found that the ratio of p-PI3K/PI3K also increased with the increase in o-HA concentration, suggesting that the o-HA viscous solution may activate the PI3K signaling pathway. However, to confirm this conclusion, it is necessary to verify that the ratio of the downstream key molecule p-AKT/AKT also increases (Figure 9).

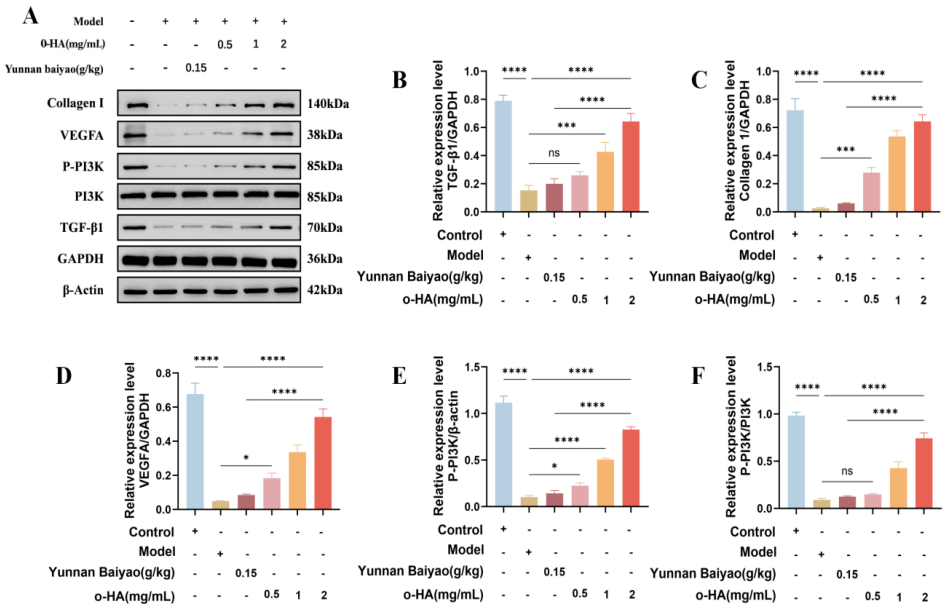

Figure 9: Western blotting is employed to detect the expression of proteins associated with skin healing. A: Expression of Collagen I, TGF-β1, VEGFA, PI3K, and p-PI3K proteins in the skin wound tissue of C57BL mice. B-D: Compared with the model group, the gray value ratios of Collagen I, VEGFA, and TGF-β1 to GAPDH in the positive drug group and the o-HA viscous solution group increased, indicating an upregulation of the expression of the target proteins Collagen I, VEGFA, and TGF-β1. E: Compared with the model group, the ratio of p-PI3K/β-Actin in the positive drug group and the o-HA viscous solution group increased, indicating that the relative content of phosphorylated PI3K in the total protein increased. F: Compared with the model group, the grayscale ratio of p-PI3K/PI3K in the positive drug group and the o-HA viscous solution group increased, indicating that the PI3K pathway may be activated. n=3. Compared with the model group: *P<0.05, **P<0.01, ***P<0.001, ****P<0.0001.

Conclusion

This study confirms that the o-HA fragments with molecular weights ranging from 4.1 to 9.9 kDa obtained through HAase degradation can enhance the viability of 3T3 and L929 cells, improve scratch closure, and alleviate oxidative stress. Moreover, the o-HA viscous solution can promote the healing of skin wounds in C57BL mice and upregulate the expression of proteins related to

skin healing, providing experimental evidence for the development of o-HA as a wound-healing promoting material.

Credit Authorship Contribution Statement

Bo Dou: Data curation, Visualization, Formal analysis, Writing–review & editing. Shaoyuan Huang: Writing–review & editing. Ruiqi Wu: Data curation, Visualization, Formal analysis. Xueli Su: Supervision, Conceptualization. Chang Liang: Writing–review & editing. Yanru Zhu: Writing–review & editing. Changhua Hu: Supervision, Conceptualization. Xiaoqun Duan: Supervision, Funding acquisition.

Declaration of Competing Interest

The authors have no competing financial interest.

Data Availability

Data will be made available on request.

Ethic Approval and Consent to Participate

All animal experiments were conducted in accordance with protocols approved by the Animal Ethics Committee of Guilin Medical University (Approval No. GLMU-IACUC-202510110). Male C57BL mice aged 6 to 8 weeks (License No.: SCXK(Yu)2020-0005.).

Declarations

This research was supported by the Major Science and Technology Project of Guangxi, with the project number (AA23023035).

Consent for Publication

All authors read and agreed to the submission of this research work to this journal.

Acknowledgement

None.

References

1. Patrulea V, Ostafe V, Borchard G, Jordan O (2015) Chitosan as a starting material for wound healing applications. Eur J Pharm Biopharm 97(Pt B): 417-426.
2. Duan Y, Siyu Chen, Yan Wang, Zhongshuang Liu, Lansheng Wei, et al. (2026) Chiral biomaterials for promoting wound healing: Fabrication strategies, therapeutic applications, and future prospects. Colloids Surf B Biointerfaces 259: 115328.
3. Savoji H, Godau B, Hassani MS, Akbari M (2018) Skin Tissue Substitutes and Biomaterial Risk Assessment and Testing. Front Bioeng Biotechnol 6: 86.
4. Zöller N, Eva Valesky, Manuel Butting, Matthias Hofmann, Stefan Kippenberger, et al. (2014) Clinical application of a tissue-cultured skin autograft: an alternative for the treatment of non-healing or slowly healing wounds? Dermatology 229: 190-198.
5. Nunery WR (2001) Risk of prion transmission with the use of xenografts and allografts in surgery. Ophthalmic Plast Reconstr Surg 17: 389-394.
6. Ansari M, Darvishi A (2024) A review of the current state of natural biomaterials in wound healing applications. Front Bioeng Biotechnol 12: 1309541.
7. Mahdi L, Martien R, Murwanti R, Nugroho AK (2025) Review of Polysaccharides/Proteins Combine With Metals: A New Strategy for Wound Healing Therapy. Biopolymers 116(6): e70058.
8. Wang L, Zhou F, Xie W (2025) Advances in hyaluronic acid-based biomaterials: applications in cancer therapy, wound healing, and disease management. J Mater Sci Mater Med 36(1): 91.
9. Yang H, Liu Song, Bingxue Sun, Di Chu, Leilei Yang, et al. (2021) Modulation of macrophages by a paeoniflorin-loaded hyaluronic acid-based hydrogel promotes diabetic wound healing. Mater Today Bio 12: 100139.
10. Xiong F, Zainen Qin, Haimin Chen, Qiumei Lan, Zetao Wang, et al. (2020) pH-responsive and hyaluronic acid-functionalized metal-organic frameworks for therapy of osteoarthritis. J Nanobiotechnology 18(1): 139.
11. Wang X, Xiaojun Liu, Chao Li, Jiangtao Li, Meng Qiu, et al. (2025) Effects of molecular weights on the bioactivity of hyaluronic acid: A review. Carbohydr Res 552: 109472.
12. Li J, Meng Qiao, Yuan Ji, Lei Lin, Xing Zhang, et al. (2025) Chemical, enzymatic and biological synthesis of hyaluronic acids. Int J Biol Macromol 152: 199-206.
13. Pujol Martí J, Müller Lierheim WGK (2025) Very High Molecular Weight Hyaluronic Acid as an Enhanced Vehicle in Therapeutic Eye Drops: Application in a Novel Latanoprost Formulation for Glaucoma. Bioengineering (Basel) 12(9): 907.
14. Adam D, Emilie Luczka Majérus, Julie Cellier, Charline Dos Santos Dietz, Claire Kileztky, et al. (2025) Low-molecular-weight hyaluronic acid improves regeneration of cystic fibrosis airway epithelium. ERJ Open Res 11(4): 00799-2024.
15. D Agostino M, Giori AM, Vassallo V, Schiraldi C, D Agostino A (2025) Protective and Anti-Inflammatory Effect of Novel Formulation Based on High and Low Molecular Weight Hyaluronic Acid and Salvia haenkei. Int J Mol Sci 26(3): 1310.
16. Chen C, Henan Zhang, Jingjun Han, Lin Yang, Shuang Li, et al. (2025) Synthesis and antitumor activity of ultra-low molecular weight hyaluronic acid-decorated camptothecin conjugates. Carbohydr Polym 351: 123144.
17. He C, Wang R, Zhang Q, Wang Y, Huang N (2025) In Vitro Bioactivity of a Recombinant Human Collagen Peptide in a Filler Biomimetic Skin Model. J Cosmet Dermatol 24(12): e70592.
18. Lee BM, Park SJ, Noh I, Kim CH (2021) The effects of the molecular weights of hyaluronic acid on the immune responses. Biomater Res 25(1): 27.
19. Tian Z, Jiang F, Cong H, Zhu S (2023) Molecular weight determination of low molecular weight hyaluronic acid and chondroitin sulfate by gel permeation chromatography. Carbohydr Polym 311:120488.
20. Huang YC, Kuen Yu Huang, Wei Zhen Lew, Kang Hsin Fan, Wei Jen Chang, et al. (2019) Gamma-Irradiation-Prepared Low Molecular Weight Hyaluronic Acid Promotes Skin Wound Healing. Polymers (Basel). 11: 1214.
21. Heo TH, Bon Kang Gu, Kyungeun Ohk, Jeong Kee Yoon, Young Hoon Son, et al. (2025) Polynucleotide and Hyaluronic Acid Mixture for Skin Wound Dressing for Accelerated Wound Healing. Tissue Eng Regen Med 22(4): 515-526.
22. Čejka Č, Jacques Luyckx, Taras Ardan, Jan Plátenník, Jakub Širc, et al. (2010) The effect of actinoquinol with hyaluronic acid in eye drops

on the optical properties and oxidative damage of the rabbit cornea irradiated with UVB rays. Photochem Photobiol 86(6): 1294-1306.

23. Salem A, El Ghlban S, Montaser AS, F Abdelhameed M, Attia MF (2025) Enhanced Wound Healing, Anti-Inflammatory, and Anti-Oxidative Effects of Vitamin C-Loaded Hyaluronic Acid-Collagen Scaffolds in Preclinical Rat Models. ACS Biomater Sci Eng. 11(12): 7461-7473.

24. Gao Y, Yao Sun, Hao Yang, Pengyu Qiu, Zhongcheng Cong, et al. (2019) A Low Molecular Weight Hyaluronic Acid Derivative Accelerates Excisional Wound Healing by Modulating Pro-Inflammation, Promoting Epithelialization and Neovascularization, and Remodeling Collagen 20: 3722.

25. Uminska W, Fekner Z, Kasinski D, Pokrywczynska M (2025) Extracellular vesicles from mesenchymal stem/stromal cells as emerging tools in wound healing: mechanisms and therapeutic potential. Stem Cell Res Ther 17: 21.

26. López Cánovas AE, Victoria Sanes M, Martínez Hernández GB, López Gómez A (2025) Methods for Determining the High Molecular Weight of Hyaluronic Acid: A Review. Polymers (Basel) 17: 3289.

27. Arakawa T, Masataka Nakagawa, Chiaki Sakuma, Yui Tomioka, Yasunori Kurosawa, et al. (2024) Polysaccharide as a Separation Medium for Gel Electrophoresis. Polysaccharides 5: 380-398.

28. Mayes EL (1984) Determination of protein molecular weights by gel permeation high pressure liquid chromatography. Methods Mol Biol 1: 5-12.

29. Drozdova M, Marina Vodyakova, Tatiana Tolstova, Marina Chernogortseva, Nikita Sazhnev, et al. (2023) Composite Hydrogels Based on Cross-Linked Chitosan and Low Molecular Weight Hyaluronic Acid for Tissue Engineering. Polymers (Basel). 15(10): 2371.

30. Goldberg RL, Toole BP (1987) Hyaluronate inhibition of cell proliferation. Arthritis Rheum 30(7): 769-778.

31. Liu J, Wang BY, Liu CH, Yang C, Zhao BT (2024) Proteomic analysis reveals the mechanism that low molecular weight hyaluronic acid enhances cell migration in keratinocyte. J Pharm Biomed Anal 250: 116402.

32. Giometti FC, Caroline LK, Malheiros LAC, Jacobo HM, Andrade SMH (2022) Oxidized hyaluronic acid/adipic acid dihydrazide hydrogel as cell microcarriers for tissue regeneration applications.e-Polymers. 22: 949-958.

33. Liu J, Piao M, Li Y, Yang C, Zhao B (2025) The key role of hyaluronic acid molecular weight in HIF-1α pathway-mediated hypoxic microenvironment reprogramming. Int J Biol Macromol 321(Pt 3): 146506.

34. Romero FJ, F Bosch Morell, M J Romero, E J Jareño, B Romero, et al. (1998) Lipid peroxidation products and antioxidants in human disease. Environ Health Perspect 106(Suppl 5(Suppl 5)): 1229-1234.

35. Jomova K, Suliman Y Alomar, Saleh H Alwasel, Eugenie Nepovimova, Kamil Kuca, et al. (2024) Several lines of antioxidant defense against oxidative stress: antioxidant enzymes, nanomaterials with multiple enzyme-mimicking activities, and low-molecular-weight antioxidants. Arch Toxicol 98(5): 1323-1367.

36. Zhang M (2025) Saccharomyces cerevisiae fermentation of high molecular weight hyaluronic acid enhanced the antioxidant capacity in skin fibroblasts. Arch Microbiol 207: 66.

37. Campo GM, Angela Avenoso, Salvatore Campo, Angela D Ascola, Alida M Ferlazzo, et al. (2004) Reduction of DNA fragmentation and hydroxyl radical production by hyaluronic acid and chondroitin-4-sulphate in iron plus ascorbate-induced oxidative stress in fibroblast cultures. Free Radic Res 38(6): 601-611.

38. Huang YC (2019) Gamma-Irradiation-Prepared Low Molecular Weight Hyaluronic Acid Promotes Skin Wound Healing. Polymers (Basel) 11: 1214.

39. Stewart DC, Becky K Brisson, William K Yen, Yuchen Liu, Chao Wang, et al. (2025) Type III Collagen Regulates Matrix Architecture and Mechanosensing during Wound Healing. J Invest Dermatol 145: 919-938.

40. Sohutskay DO, Buganza Tepole A, Voytik Harbin SL (2021) Mechanobiological wound model for improved design and evaluation of collagen dermal replacement scaffolds. Acta Biomater 135: 368-382.

41. Cullen B, Gefen A (2023) The biological and physiological impact of the performance of wound dressings. Int Wound J 20(4): 1292-1303.

42. Eremenko EE, Kwan PO, Ding J, Ghosh S, Tredget EE (2024) The effects of TGF-β1 and IFN-α2b on decorin, decorin isoforms and type I collagen in hypertrophic scar dermal fibroblasts. Wound Repair Regen 32(2): 135-145.

43. Chattopadhyay S, Teixeira LBC, Kiessling LL, McAnulty JF, Raines RT (2022) Bifunctional Peptide that Anneals to Damaged Collagen and Clusters TGF-β Receptors Enhances Wound Healing. ACS Chem Biol 17(2): 314-321.

44. Li Z, Leyang Zhang, Yang Wang, Yifu Zhu, Haomiao Shen, et al. (2025) LA-peptide Hydrogel-Regulation of macrophage and fibroblast fates and their crosstalk via attenuating TGF-β to promote scarless wound healing. Bioact Mater 47: 417-431.

45. Palomeque Chávez JC, Matthew McGrath, Cian O Connor, Adrian Dervan, James E Dixon, et al. (2025) Development of a VEGF-activated scaffold with enhanced angiogenic and neurogenic properties for chronic wound healing applications. Biomater Sci 13(8): 1993-2011.

46. David Raoudi M, Frédéric Tranchepain, Brigitte Deschrevel, Jean Claude Vincent, Patrick Bogdanowicz, et al. (2008) Differential effects of hyaluronan and its fragments on fibroblasts: relation to wound healing. Wound Repair Regen 16(2): 274-287.

47. Chen Y, Qing Wang, Fangrui Ning, Chang Du, Mingsheng Chen, et al. (2024) Dynamic Hyaluronic Acid Hydrogels for Comprehensively Regulating Inflammation, Angiogenesis, and Metabolism to Effectively Proheal Diabetic Wounds. ACS Appl Mater Interfaces 16(51): 70256-70273.